Astronomy & Astrophysics manuscript no. CS+O_final
October 7, 2020

Gas phase Elemental abundances in Molecular cloudS (GEMS)

III. Unlocking the CS chemistry: the CS+O reaction

Niyazi Bulut[1], Octavio Roncero[2], Alfredo Aguado[3], Jean-Christophe Loison[4], David Navarro-Almaida[5], Valentine Wakelam[6], Asunción Fuente[5], Evelyne Roueff[7], Romane Le Gal[8], Paola Caselli[9], Maryvonne Gerin[7], Kevin M. Hickson[6], Silvia Spezzano[9], P. Riviére-Marichalar[5], T. Alonso-Albi[5], R. Bachiller[5], Izaskun Jiménez-Serra[10], C. Kramer[11], Belén Tercero[5,12], Marina Rodriguez-Baras[5], S. García-Burillo[5], Javier R. Goicoechea[2], S. P. Treviño-Morales[13], G. Esplugues[5], S. Cazaux[14], B. Commercon[15], J. Laas[9], J. Kirk[16], V. Lattanzi[9], R. Martín-Doménech[8], G. Muñoz-Caro[10], J. Pineda[9], D. Ward-Thompson[16], M. Tafalla[5], N. Marcelino[2], J. Malinen[17,18], R. Friesen[19], B. M. Giuliano[9], M. Agúndez[2], and A. Hacar[20]

[1] University of Firat, Department of Physics, 23169 Elazig, Turkey
[2] Instituto de Física Fundamental (IFF-CSIC), C.S.I.C., Serrano 123, 28006 Madrid, Spain.
[3] Departamento de Química-Física Aplicada, Unidad asociada IFF-UAM, Universidad Autónoma de Madrid, 28049 Spain
[4] Institut des Sciences Moléculaires ISM), CNRS, Univ. Bordeaux, 351 cours de la Libération, F-33400, Talence, France
[5] Observatorio Astronómico Nacional (IGN), c/ Alfonso XII 3, 28014 Madrid, Spain.
[6] Laboratoire d'astrophysique de Bordeaux, Univ. Bordeaux, CNRS, B18N, allée Geoffroy Saint-Hilaire, 33615 Pessac, France
[7] Sorbonne Université, Observatoire de Paris, Université PSL, CNRS, LERMA, F-92190, Meudon, France
[8] Center for Astrophysics | Harvard & Smithsonian, 60 Garden St., Cambridge, MA 02138, USA
[9] Centre for Astrochemical Studies, Max-Planck-Institute for Extraterrestrial Physics,Giessenbachstrasse 1, 85748, Garching, Germany
[10] Centro de Astrobiología (CSIC-INTA), Ctra. de Ajalvir, km 4, Torrejón de Ardoz, 28850 Madrid, Spain
[11] Instituto Radioastronomía Milimétrica (IRAM), Av. Divina Pastora 7, Nucleo Central, 18012, Granada, Spain
[12] Observatorio de Yebes (IGN), Cerro de la Palera s/n, 19141 Yebes, Guadalajara, Spain.
[13] Chalmers University of Technology, Department of Space, Earth and Environment, SE-412 93 Gothenburg, Sweden
[14] Faculty of Aerospace Engineering, Delft University of Technology, Delft, The Netherlands ; University of Leiden, P.O. Box 9513, NL, 2300 RA, Leiden, The Netherlands
[15] École Normale Supérieure de Lyon, CRAL, UMR CNRS 5574, Université Lyon I, 46 Allée d'Italie, 69364, Lyon Cedex 07, France
[16] Jeremiah Horrocks Institute, University of Central Lancashire, Preston PR1 2HE, UK
[17] Department of Physics, University of Helsinki, PO Box 64, 00014 Helsinki, Finland
[18] Institute of Physics I, University of Cologne, Cologne, Germany
[19] National Radio Astronomy Observatory, 520 Edgemont Rd., Charlottesville VA 22901, USA
[20] Leiden Observatory, Leiden University, PO Box 9513, 2300-RA, Leiden, The Netherlands

October 7, 2020

ABSTRACT

Context. CS is among the most abundant gas phase S-bearing molecules in cold dark molecular clouds. It is easily observable with several transitions in the millimeter wavelength range, and it has been widely used as a tracer of the gas density in the interstellar medium in our Galaxy and external galaxies. However, chemical models fail to account for the observed CS abundances when assuming the cosmic value for the elemental abundance of sulfur.
Aims. The CS+O → CO + S reaction has been proposed as a relevant CS destruction mechanism at low temperatures that could explain the discrepancy between models and observations. Its reaction rate has been experimentally measured at temperatures of 150−400 K, but the extrapolation to lower temperatures is doubtful. Our goal is to calculate the CS+O reaction rate at temperatures <150 K which are prevailing in the interstellar medium.
Methods. We have performed *ab initio* calculations to obtain the three lowest Potential Energy Surfaces (PES) of the CS +O system. These PES's are used to study the reaction dynamics, using several methods, classical, quantum and semiclassical to eventually calculate the CS + O thermal reaction rates. In order to check the accuracy of our calculations, we compare the results of our theoretical calculations for T∼150−400 K, with those obtained in laboratory.
Results. Our detailed theoretical study on the CS+O reaction which is in agreement with the experimental data obtained at 150-400 K, showing the reliability of our approach. After a careful analysis at lower temperatures we find that the rate constant at 10 K is negligible, below 10^{-15} cm^3 s^{-1}, consistent with the extrapolation of experimental data using the Arrhenius expression.
Conclusions. Our theoretical results show that the CS+O reaction is negligible at the typical low temperature of the cold interstellar medium. We discuss possible scenarios to explain the abundance of CS and HCS^+ in the prototypical dark cloud TMC 1.

1. Introduction

Gas-phase chemistry plays a key role in the star formation process through critical aspects such as the gas cooling and the ionization fraction. Molecular filaments can fragment into prestellar cores to a large extent because molecules cool the gas, thus diminishing the thermal support relative to self-gravity. The ion-

ization fraction controls the coupling of magnetic fields with the gas, driving the dissipation of turbulence and angular momentum transfer, therefore playing a crucial role in protostellar collapse and accretion disk dynamics (see Zhao et al. 2016; Padovani et al. 2013). In particular, atomic carbon (C) is the main donor of electrons in the cloud surface (A_V < 4 mag) and, because of its lower ionization potential, and as long as it is not heavily depleted, Sulfur (S) becomes then the main electron provider at higher extinctions. In the absence of other ionization agents (X-rays, UV photons, J-type shocks), the ionization fraction is a function of the cosmic-ray ionization rate for H_2 molecules, ζ_{H_2}, and of the elemental gas-phase abundances (McKee 1989; Caselli et al. 2002).

Gas phase Elemental abundances in Molecular CloudS (GEMS) is an IRAM 30m Large Program aimed at estimating the S, C, N, O depletions and the gas ionization fraction, $X(e^-)=n_{e^-}/n_H$, as a function of visual extinction in a selected set of prototypical star-forming filaments in low-mass (Taurus), intermediate-mass (Perseus), and high-mass (Orion) star forming regions. Determining sulfur depletion is probably the most challenging goal of this project because the sulfur chemistry in cold dark clouds remains a puzzling astrochemical problem. A few sulfur compounds have been detected in diffuse clouds suggesting that the sulfur abundance in these low density regions is close to the cosmic value (Neufeld et al. 2015). However, sulfur seems to be depleted in molecular clouds by a factor of ∼3−100 compared to its estimated cosmic abundance (Tieftrunk et al. 1994; Ruffle et al. 1999; Goicoechea et al. 2006; Fuente et al. 2019; Vidal et al. 2017; Laas & Caselli 2019; Shingledecker et al. 2020). The depletion of sulfur is observed not only in cold prestellar cores, but also in hot cores or corinos, where the icy grain mantles are expected to evaporate (Esplugues et al. 2014; Vidal & Wakelam 2018), and in bipolar outflows (Wakelam et al. 2005; Holdship et al. 2016). Chemical models predict that the two main sulfur reservoirs are atomic S and solid organosulfur coumpounds, mainly H_2S but also the species like OCS (Vidal et al. 2017; Laas & Caselli 2019), but the direct observation of these species remains difficult. Alternatively, a significant fraction of sulfur can be trapped in allotropic form, the most abundant of which being S_4 (Shingledecker et al. 2020), as also found in laboratory experiments (e.g. Jiménez-Escobar & Muñoz Caro (2011)); S allotropes can also be an important sink of sulfur in comets (e.g. Calmonte et al. (2016)). Thus far, there are only upper limits of the solid H_2S abundance in the interstellar medium (Jiménez-Escobar & Muñoz Caro 2011). Atomic S has only been detected in some bipolar outflows using the infrared space telescope Spitzer (Anderson et al. 2013). Thus, we need to base our estimation of the sulfur elemental abundance on the observation of minor species and the use of progressively more complex gas-grain chemical models (see e.g. Holdship et al. 2016; Vidal et al. 2017; Navarro-Almaida et al. 2020; Laas & Caselli 2019; Shingledecker et al. 2020).

The chemistry of sulfur is still poorly understood with large uncertainties in the gas phase and surface chemical network. However, a large theoretical and observational effort has been undertaken in the last five years to understand sulfur chemistry, progressively leading to a new paradigm (Fuente et al. 2016; Vidal et al. 2017; Le Gal et al. 2019; Laas & Caselli 2019; Navarro-Almaida et al. 2020; Shingledecker et al. 2020). Based on 'ab initio' calculations, Fuente et al. (2016) determined the rate of the key reaction $S+O_2 \rightarrow SO+O$ at low temperatures. Using this updated gas-phase chemical network, they concluded that a moderate S depletion, $S/H \sim (0.6 - 1.0) \times 10^{-6}$, is necessary to reproduce the high abundances of S-bearing species observed in the dense core Barnard 1b. This depletion was significantly lower than the usual values adopted in dark clouds (Ruffle et al. 1999; Agúndez & Wakelam 2013) and some explanations were proposed to explain this overabundance of S-bearing species such as a rapid collapse (∼ 0.1 Myr) that allows most S- and N-bearing species to remain longer in the gas phase, or the interaction of the dense gas with the compact outflow associated with B1b-S. The whole gas-phase sulfur chemical network was revised by Vidal et al. (2017) by looking systematically at the possible reactions between S and S^+ with the most abundant species in dense molecular clouds (CO, CH_4, C_2H_2, and c-C_3H_2) as well as the potential reactions between sulfur compounds and the most abundant reactive species in molecular clouds (C, C^+, H, N, O, OH, and CN). They used this new chemical network to interpret previous observations towards the prototypical dark core TMC1- CP and found that the best fit to the observations was obtained when adopting the cosmic sulfur abundance as the initial condition, and an age of ∼1 Myr. Using the same chemical network but with 1D modeling, Vastel et al. (2018) tried to fit the abundances of twenty-one S-bearing species towards the starless core L1544. The authors found that it was impossible to fit all the species with the same sulfur abundance, with variations of a factor of 100, being models with initial $S/H \sim 8.0 \times 10^{-8}$ those who best fitted the abundances of all the twenty-one species. New calculations of the $SO + OH \rightarrow SO_2 + H$ reaction rate reported in Fuente et al. (2019) improved the description of the SO chemistry at the low temperatures prevailing in dark clouds. Adopting this new rate and using observations from the GEMS project, Fuente et al. (2019) derived a sulfur gas-phase abundance of $S/H \sim (0.4 - 2.2) \times 10^{-6}$ to account for the observations in the translucent gas ($n(H_2) > 10^4$ cm^{-3}) towards the TMC 1 filament. In this paper, the gas-phase PDR Meudon code was used to fit the observations in the border of this prototypical cloud. Regarding surface chemistry, Laas & Caselli (2019) performed an in-depth revision of the surface chemical network in order to incorporate photochemistry, new results from laboratory, and all

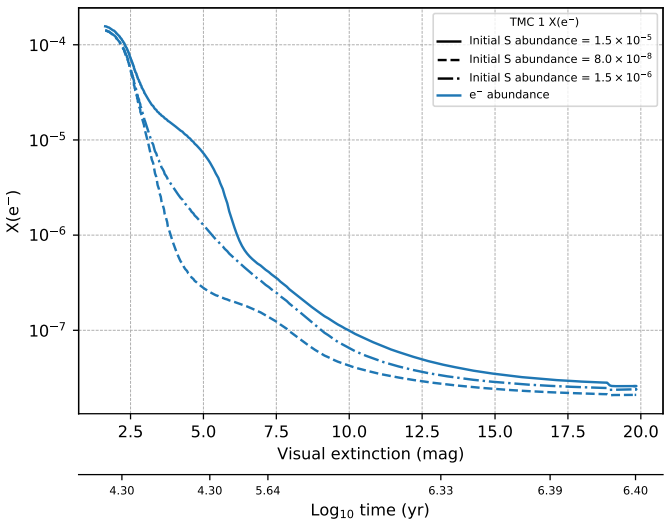

Fig. 1. Gas ionization fraction, $X(e^-)$, as a function of the visual extinction assuming different values of the initial sulfur elemental abundance in TMC 1. The calculations have been performed using the gas-grain chemical code Nautilus (Ruaud et al. 2016), with the physical structure and the updated chemical network described in Navarro-Almaida et al. (2020)

the S-bearing molecules detected so far. With this new model, they improved the agreement between observations and model predictions assuming the cosmic sulfur abundance. In this line of a more accurate description of the surface chemistry, Shingledecker et al. (2020) examined the effects of introducing cosmic ray-driven radiation chemistry, and fast non-diffusive bulk reactions for radicals and reactive species on the sulfur surface chemistry. They showed that these changes have a great impact on the abundances of sulfur-bearing species in ice mantles, in particular a reduction in the abundance of solid-phase H_2S and HS, and a significant increase in the abundances of OCS, SO_2, and allotropes of sulfur such as S_8.

GEMS provides a complete (the most abundant species) and spatially resolved (measurements at different visual extinctions within the same cloud down to $A_V \sim 3$ mag) database of sulfur bearing species, which allows extensive comparison with models to describe the progressive sulfur depletion along the cloud, and, eventually, to estimate the initial S/H. Navarro-Almaida et al. (2020) carried out a detailed physical and chemical modeling of the cores TMC1-CP, TMC1-C and Barnard 1b, in an attempt to explain the observed CS, SO and H_2S observations, which are the most abundant gas-phase S-bearing species present in these clouds. To do so, Navarro-Almaida et al. (2020) used the chemical model Nautilus, recently updated by Le Gal et al. (2019) to include the most recent observations, reaction coefficient rates and S-chemical pathways (Fuente et al. 2016, 2017; Vidal et al. 2017; Fuente et al. 2019). In addition, Navarro-Almaida et al. (2020) incorporated in this model the new surface reaction network by Laas & Caselli (2019). Finally, they took into account chemical desorption using the prescriptions of Minissale et al. (2016) for bare and ice-coated grains. One of the results of that paper was that they were unable to fit the CS, SO and H_2S abundances, simultaneously. While the SO and H_2S abundances were well fitted with their chemical model assuming the cosmic Sulfur elemental abundances, the CS abundance was over-estimated by a factor >10. This lack of accordance prevents us from determining a reliable value of the initial S/H abundance which remained with an uncertainty of a factor of > 10, varying between S/H $\sim 10^{-6}$ to 1.5×10^{-5}. They recall that different initial S/H abundances would lead to a different gas ionization fraction. In Fig 1, we predict X(e^-) using the chemical model described by Navarro-Almaida et al. (2020) and different initial values of S/H. It should be noticed X(e^-) varies by more than a factor of 10 for A_V< 10 mag, depending of the initial value of S/H, which becomes a key parameter to model the fragmentation of molecular filaments to form dense cores.

2. CS chemical network

CS is among the most abundant gas phase S-bearing molecules in dark clouds. It is easily observable with several transitions in the millimeter wavelength range, and has a simple rotational spectrum with well known collisional coefficients (Denis-Alpizar et al. 2018; Lique et al. 2006). Therefore, it has been largely used as density and column density tracer in the interstellar medium in our Galaxy and external galaxies (see, e.g. Snell et al. 1984; Lapinov et al. 1998; Kim et al. 2020; Martín et al. 2005; Bayet et al. 2009; Kelly et al. 2015). Moreover, CS is the only S-bearing molecule routinely detected in protoplanetary disks and therefore the main tracer of the sulfur abundance in the primordial material to form planets (Agúndez et al. 2018; Le Gal et al. 2019). An understanding of CS chemistry is essential for the correct interpretation of the observations from all astrophysical environments. Unfortunately, chemical models do a poor job accounting for these observations, usually predicting CS abundances much larger than those observed (Gratier et al. 2016; Vidal et al. 2017).

The chemistry of CS in interstellar clouds is closely correlated with that of HCS^+ and involves reactions that have never been studied experimentally, leading to large uncertainties. For very young molecular clouds, where the ionization fraction from the diffuse period is still very large, sulfur is essentially in atomic ionized form and controls the chemistry of sulfur (e.g. Goicoechea et al. (2006)). CS is then produced essentially from the electronic dissociative recombination (DR) of HCS^+, HCS^+ being produced by the $S^+ + CH_2$ and $CS^+ + H_2$ reactions, CS^+ being produced by the ion-neutral reactions $S^+ + CH$ and $S^+ + C_2$. For the more advanced stages of dense clouds, which probably correspond much more to the clouds observed in the GEMS project, the ionic fraction is much lower and the sulfur is mainly in neutral atomic form (the reactions of ionized atomic sulfur are not negligible but play a secondary role). Under these conditions, although the DR of HCS^+ still produces CS, HCS^+ is also mostly formed from CS (either directly by the $CS + H_3^+$ reaction, or indirectly by $CS + H^+ \rightarrow H + CS^+$ followed by $CS^+ + H_2 \rightarrow HCS^+ + H$) and not from S^+ reactions. In that case CS is produced by neutral reactions, mainly S + CH and $S + C_2$, with secondary contributions by H + HCS, $S + CH_2$ and C + SO. The overestimation of CS in the models versus the observations could come from an underestimation of the rates of consumption reactions (mainly $CS + H^+$ and $CS + H_3^+$). This seems however unlikely because even if there are no measurements, the rates used are those resulting from the capture theory and thus close to the maximum theoretical rates. The CS overestimation could also come from the overestimation of the production rates from neutral reactions such as S + CH and $S + C_2$, or from missing consumption reactions of CS. For the latter case, Vidal et al. (2017) suggested that a high rate for the reaction of CS with the abundant atomic oxygen, O + CS, will decrease the overproduction of CS without heavily affecting the abundance of the S-bearing molecules, except for the chemically related HCS^+. This possibility has motivated this work to better quantify the O + CS reaction rate.

Chemical models use the CS + O reaction rate constants measured by Lilenfeld & Richardson (1977) in the 150-300 K interval, considerably higher than the typical T_k~10 K of dark clouds, extrapolated to low temperatures using the Arrhenius expression. The extrapolation to lower temperatures is always questionable and an experimental measurement and/or theoretical calculations are needed to confirm these values. González et al. (1996) did theoretical simulations, by calculating the potential energy surface (PES) for the ground and first excited states, and obtained reaction rate constants under several transition state theory (TST) approaches. Their results at 150−300 K were, however, considerably lower than the experimental measurements casting doubts about the accuracy of the calculated rates. It is, therefore, necessary to improve the theoretical simulations to predict reasonable reaction rates at the lower temperatures, prevailing in the interstellar medium (ISM).

This study is devoted to the theoretical determination of the CS+O reaction rate. The *ab initio* calculations performed to produce the lower potential energy surfaces (PES) are described in Section 3. These PES's are then used to study the reaction dynamics, using several methods, classical, quantum and semiclassical to derive the reaction rates. Finally, we test the role of the new reaction rates on realistic chemical models of cold dark clouds.

3. Potential energy surfaces

The calculation of the PES is a mandatory step for any dynamical study of a chemical reaction. The reaction

$$CS(X^1\Sigma^+) + O(^3P) \rightarrow CO(X^1\Sigma^+) + S(^3P) \quad (1)$$

involves open shell atoms in reactants and products, presenting 3 degenerate electronic states at long distances (neglecting spin-orbit), correlating to P states of the oxygen or sulfur atoms. At long distances the energy of these three states are dominated by the dipole-quadrupole interactions (Buckingham 1967). At short distances, however, there are excited electronic states, correlating to $CS(a^3\Pi) + O(^3P)$ (González et al. 1996), which cross with the lower electronic manifold, giving rise to the formation of the $CO(X^1\Sigma^+) + S(^3P)$ products. These crossings give rise to small barriers, whose height strongly depends on the electronic basis and the method chosen to describe the electronic correlation, as noted by González et al. (1996).

In this work accurate *ab initio* calculations are performed using the internally contracted multireference configuration interaction (ic-MRCI) method (Werner & Knowles 1988a,b) including the Davidson correction (icMRCI+Q) (Davidson 1975). In these calculations, the molecular orbitals are optimized using a state-averaged complete active space self-consistent field (SA-CASSCF) method, with an active space of 14 orbitals (11 and 3 of a' and a'' symmetry, respectively). One $^3A'$ and two $^3A''$ electronic states are calculated and simultaneously optimized. In all these calculations the aug-cc-pVTZ basis set is used (Dunning & Jr. 1989). For the ic-MRCI calculations, 7 orbitals are kept doubly occupied, giving rise to $\approx 30 \times 10^6$ (6500×10^6) contracted (uncontracted) configurations. All *ab initio* calculations were performed with the MOLPRO suite of programs (Werner et al. 2012).

The analytical representation of the adiabatic PESs is done in three parts:

1. For short-intermediate distances, a three-dimensional cubic spline method is used with the DB3INK/DB3VAL subroutines based on the method of de Boor (1978) and distributed by GAMS (Boisvert 2015). A dense grid is calculated, composed by 20×14×19 points in the intervals defined in bond coordinates as: R_{CO} ([0.9, 10] Å), the R_{CS} ([1, 7] Å), Θ_{OCS} ([0, π]), respectively.
2. At long distances ($R_{CO} > 8$ Å), dipole-quadrupole long range interactions are considered using the expressions defined by Zeimen et al. (2003) in reactant Jacobi coordinates. The V(R_{CS}) obtained at R_{CO}=100 Å is fitted using the diatomic terms of Aguado & Paniagua (1992). The CS electric dipole is fitted as a function of the R_{CS} distance, and the $O(^3P)$ quadrupole is calculated as energy derivatives using different homogeneous electric fields (Werner et al. 2012). The long range behavior is checked by doing ic-MRCI calculations for distances R longer than 10 Å, with R being the distance between the CS center of mass and the oxygen atom.
3. In order to guarantee a continuous behavior between the previous two regions, points calculated with the long-range expression are added at R_{CO}=7, 8 and 9 Å, and a damping function among the two regions is centered at 5 Å.

The minimum energy path for the reaction is shown in Fig. 2 for the three adiabatic states ($1\ ^3A'$ and $2\ ^3A''$). The reaction is exothermic by $\approx$ 3.9 eV, in agreement with the value of 3.93 eV, reported by González et al. (1996). When zero-point energy (ZPE) is taken into account the exothermicity reduces to 3.59 eV in rather good agreement with the experimental value of 3.64 eV (Lilenfeld & Richardson 1977). The energy barriers obtained in this work are 0.043, 0.058 and 0.888 eV for the 1^3A', 1^3A" and $2^3A''$ states, respectively. These values are lower than those obtained by González et al. (1996), probably because the electronic correlation introduced by ic-MRCI is higher than the PUMP4 method.

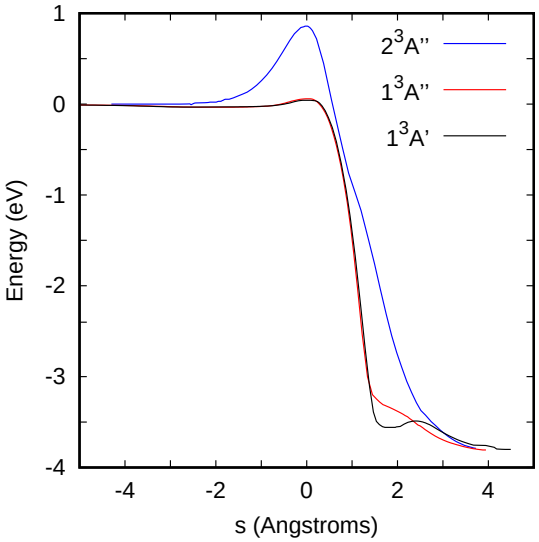

Fig. 2. Three lower adiabatic potential energy surfaces as a function of the intrinsic reaction coordinate (IRC) for the $CS(X^1\Sigma^+) + O(^3P) \rightarrow CO(X^1\Sigma^+) + S(^3P)$ reaction.

The main features of the present PESs are very similar to those discussed by González et al. (1996), represented in the contour plots shown in Fig. 3. The reaction barriers are located in the entrance channel, at nearly the equilibrium distance of CS, and at $R_{CO} \approx$2.25 Å for the ground electronic state. In addition, the angular cone of acceptance is also reduced as R distance becomes closer: the saddle point is located at OCS angle, $\Theta_{OCS} \approx 120^o$, and the interval is reduced to [80^o, 160^o]. According to the Polanyi rules, the early barrier suggests that translational energy will enhance the reactivity. The reduction of the angular cone of acceptance is expected to introduce some restrictions, as will be commented below, in the reaction dynamics section.

4. Reaction dynamics

The thermal reaction rate can be defined as

$$K(T) = \sum_{vje} w_{vje}(T)\, K_{vje}(T) \quad \text{with} \quad w_{vje} = \frac{e^{-E_{vje}/k_BT}}{\sum_{v'j'e'} e^{-E_{v'j'e'}/k_BT}} \quad (2)$$

where the sum is over all vibrational, rotational and electronic states of the reactants, CS($X^1\Sigma^+$, v j) + $O(^3P)$, of energy E_{vje}. $K_{vje}(T)$ are the initial state selected rate constants, which correspond to the Boltzmann average over the translational energy of the reaction cross section

$$K_{vje}(T) = \sqrt{\frac{8}{\pi\mu(k_BT)^3}} \int dE\, E\, \sigma_{vje}(E) e^{-E/k_BT}. \quad (3)$$

The cross section is obtained under the partial wave summation over the total angular momentum, J, as

$$\sigma_{vje}(E) = \frac{\pi}{(2j+1)\, k_{vj}^2(E)} \sum_{J\Omega} (2J+1)\, P^J_{vje\Omega}(E), \quad (4)$$

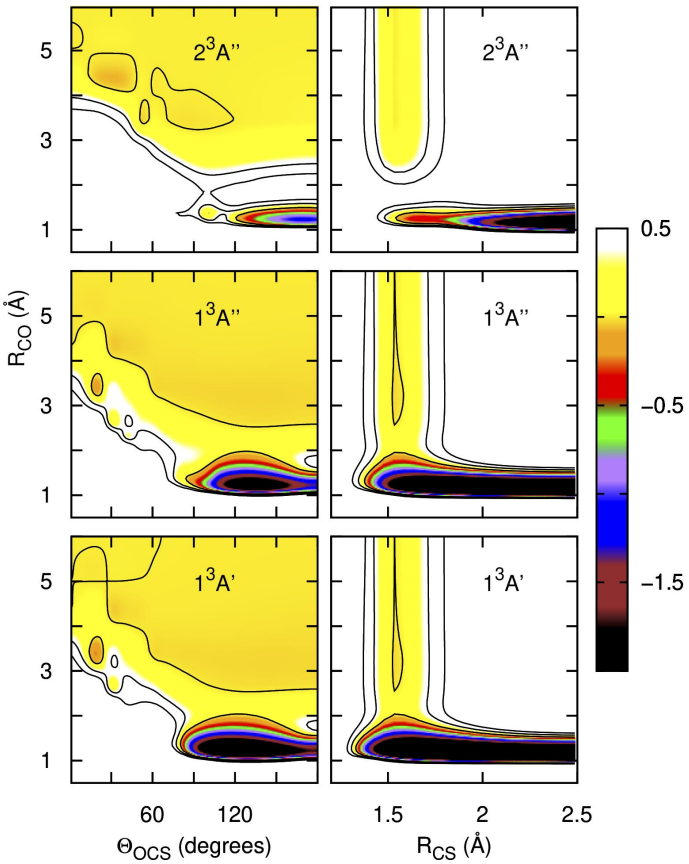

Fig. 3. Contour plots of the PES for the three electronic states obtained at the equilibrium R_{CS}= 1.535 Å as a function of R_{CO} and the OCS angle (left panels) and at an OCS angle of 120^o as a function of R_{CO} and R_{CS} distances. Energies are in eV, and the contour lines are at 0, 0.5 and 1 eV.

where $k_{vj} = \sqrt{2\mu E}/\hbar$ (with μ being the CS + O reduced mass), Ω is the helicity, *i.e.* the projection of **J** and **j** angular momenta on the z-axis of the body-fixed frame, and $P^J_{vje\Omega}(E)$ is the reaction probability for a particular initial state of the reactants, which depends on collision energy E. This quantity can be calculated with different methods, exact and approximate, quantum and classical, and below we start by determining the accuracy of each of them for J=0.

The reaction is very exothermic, but it presents a reaction barrier. It can be assumed that all the flux that passes over this barrier yields to products, reducing considerably the computational effort. This can be done using the quantum capture approach (Clary & Henshaw 1987), in which the time-independent close coupled equations (TICCE) are solved in the entrance channel, similarly to what it is done in inelastic collisions, but subject to capture conditions, *i.e.*, to outgoing complex conditions at $R < R_c$ for those channels for which E> $V_{vje\Omega}(R_c)$, R_c = 2Å, being the capture distance. Thus the TICCE are integrated from R= 2 Å to 30 Å, in the rovibrational states composed by CS(v=0,1,2) and 50 rotational states for total angular momentum J=0. This is done separately for each electronic state, $1^3A'$ and $1^3A''$ using the ZTICC code (Gómez-Carrasco et al. 2020). The capture probabilities are compared with quantum wave packet (WP) results in Fig. 4. These calculations were performed with the MADWAVE3 code (Zanchet et al. 2009) and the parameters used are listed in Table 1. The WP method is considered numerically exact, but as will be discussed below, it is very demanding computationally.

Table 1. Parameters used in the wave packet calculations in reactant Jacobi coordinates: $r_{min} \le r \le r_{max}$ is the CS internuclear distance, $R_{min} \le R \le R_{max}$ is the distance between CS center-of-mass and the oxygen atom, $0 \le \gamma \le \pi$ is the angle between **r** and **R** vectors. The initial wave packet is described in R by a gaussian centered at $R = R_0$, and at an translational energy of $E = E_0$, and width ΔE. The total reaction probability is obtained by analyzing the total flux at $r = r_\infty$

r_{min}, r_{max} = 0.1, 10 Å	N_r=512
r_{abs}= 5 Å	
R_{min}, R_{max} = 0.001, 18Å	N_R=1024
R_{abs}= 11 Å	
N_γ = 240	in $[0, \pi]$
R_0 = 9 Å	E_0, ΔE= 0.4,0.2 eV
r_∞ = 4 Å	

Clearly the quantum capture (QC) method overestimates the reaction probability. Near the reaction threshold the QC and WP results are in rather good agreement, showing a common threshold at 0.04 and 0.06 eV for $1^3A'$ and $1^3A''$, respectively. However, above the threshold energy, the QC method gives a much larger reaction probability than the WP method. This is clear evidence that not all the flux arriving at distances R shorter than R_c go on to form CO + S products, and this situation increases with increasing collision energy.

Since the reaction involves rather heavy atoms, it may be expected that quantum effects do not play an important role. The quasi-classical trajectory (QCT) method is then an interesting alternative to simplify the computationally demanding quantum WP calculations. The comparison for J=0, in Fig. 4, shows a rather good agreement, except at threshold. The QCT method is not able to describe the first peaks appearing in the WP reaction probabilities, which can be attributed to tunneling.

To better quantify the adequacy of QCT method to describe this reaction, the total cross section has been calculated with the QCT and WP methods. In order to limit the highly demanding WP calculations for high J, the centrifugal sudden approximation (Pack 1974; McGuire & Kouri 1974) (CSA) is performed, in which only one helicity Ω is included. Also, the reaction probability is calculated for J=0, 50, 100, 150 and 180, and the reaction probabilities for the remaining J's are obtained using an interpolation based on the J-shifting approximation (Aguado et al. 1997; Zanchet et al. 2013). The comparison between the WP-CS and QCT calculations are shown in Fig. 5, and they show a reasonable good agreement below 0.2 eV, corresponding to the discussion made for the reaction probabilities obtained for J=0. However, for higher energies, the QCT cross sections are in general higher than the WP-CS ones, and the differences are larger for $1^3A'$ than for $1^3A''$. At these higher energies one would expect a better agreement between classical and quantum methods, similar to that obtained for J = 0. The larger difference can be attributed to the CS approximation made to obtain the cross section in the case of the quantum WP-CS method. In order to check this, for the 1^3A' state and J = 50, 100 and 150 we have included more helicities on the reaction probabilities, Ω = 0,1, 2, 3, 4 and 5. These new calculations, labelled as WP in Fig. 5, are larger than the WP-CS, and very close to the QCT calculations up to 0.3 eV. Above this energy more helicities Ω are needed to converge the reaction probabilities of J>100. However, these calculations are extremely demanding.

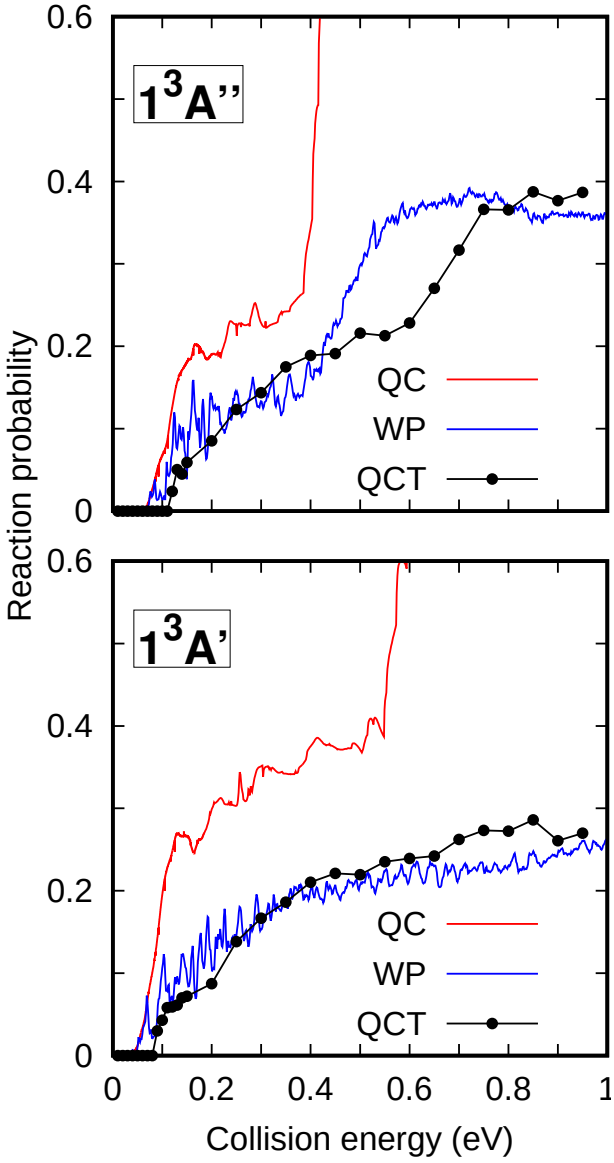

Fig. 4. CS+O → CO + S reaction probabilities versus collision energy for $J = 0$ in the 1 $^3A'$ and 1 $^3A''$ electronic states using three different methods described in the text: the quantum capture (QC) , the quantum wave packet (WP) and the quasi-classical trajectory (QCT) methods.

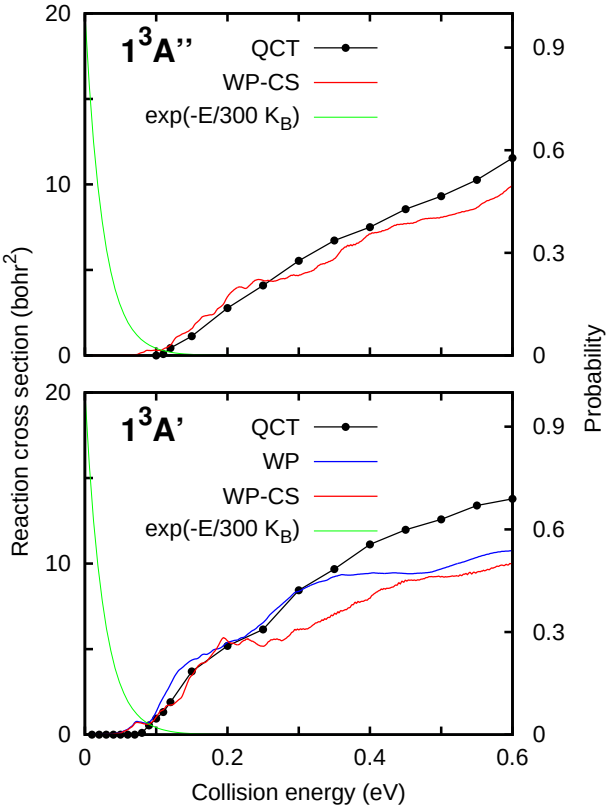

Fig. 5. CS+O → CO + S reaction cross section (in Bohr^2) versus collision energy for 1 $^3A'$ and 1 $^3A''$ electronic states using the quantum wave packet within the CS approach (WP-CSA) and the quasi-classical trajectory (QCT) methods. The energy distribution of a Boltzmann distribution for a temperature of 300 K is also shown in green. For the 1 $^3A'$, WP labels the wave-packet calculations performed including Ω=0,1,2,3,4 and 5.

In Fig. 5 the probability arising for a Boltzmann distribution at 300 K is also displayed, showing that only collision energy below 0.12 eV contribute for temperatures below 300 K. Below 0.12 eV, QCT results are lower than the quantum wave packet values. This indicates that it is important to include quantum effects near the threshold. WP methods require to do individual calculations for each initial state, and many rotational states have to be considered (which contribute significantly below 0.12 eV) because of the low rotational constant of CS. This makes the use of the WP method very computationally demanding to evaluate the thermal rate constants for this reaction, and some alternative method should be used.

Ring polymer molecular dynamics (RPMD) is a semiclassical method based on path integral methods that include quantum effects such as zero-point energy and tunneling proposed by Craig & Manolopoulos (2004). RPMD has been successfully applied to calculate reaction rate constants (Craig & Manolopoulos 2005a,b; Suleimanov et al. 2011) as recently reviewed by Suleimanov et al. (2016). Here we apply a direct version of this method recently applied to reactions of poly-atomic molecules at low temperature (Suleimanov et al. 2018; del Mazo-Sevillano et al. 2019; Bulut et al. 2019) and implemented in the code dRPMD.

RPMD and QCT results are compared in Fig. 6 for the 1 $^3A'$ and 1 $^3A''$ electronic states. The QCT calculations consist of more than 10^5 trajectories per temperature (for low temperatures more than 10^6 trajectories were needed to get convergence). RPMD results are based on 10^4 trajectories using a variable number of beads (64 for 300 K, 128 for 150 K, etc). RPMD rate constants are always about 10 times larger than the QCT ones. This is explained by the difference found in the cross section obtained with quantum WP and QCT methods at energies below 0.12 eV. RPMD includes quantum effects and is more accurate than the QCT results. It is important to stress here that, according to QC calculations, the reaction probability at low energies increases with increasing the initial rotational state of the CS reagent. The QCT and RPMD rate calculations include this effect by considering the rotational temperature, and this produces an amplification of the difference between QCT and RPMD rate constants. In both cases, many trajectories have been run for temperatures below 100 K, but no reactive ones were found. This indicates that the reaction rate constants below 100 K is very small.

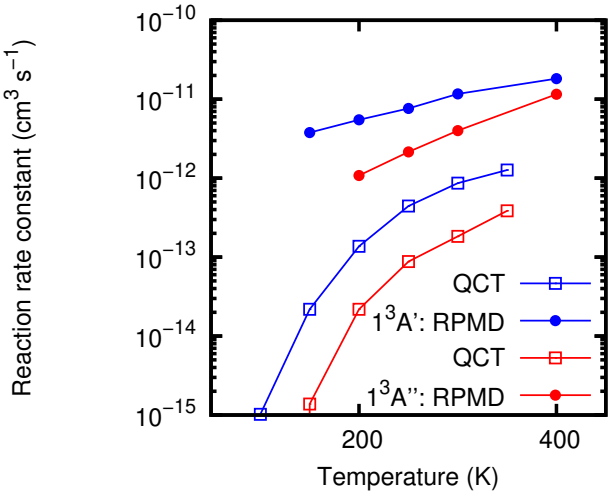

Fig. 6. CS+O → CO + S reaction rate constants obtained with RPMD (full circles) and QCT (open squares) for the $1^3A'$ (blue) and $1^3A''$ (red) electronic states.

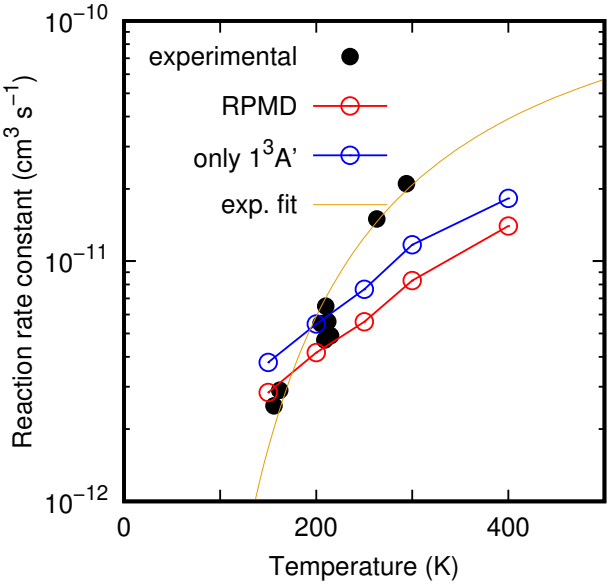

Fig. 7. Comparison of the calculated thermal rate constant for the CS+O → CO + S reaction including spin-orbit splitting and the experimental measurements of Lilenfeld & Richardson (1977). The rate constant obtained for $1^3A'$ is included for discussion. The experimental results are fit to k=A $e^{-C/T}$, with A=2.6 10^{-10} cm^{3}s^{-1} and C=757.7 K=0.065 eV.

The thermal rate constant is finally obtained by an average over the spin-orbit electronic states of O(^3P) as

$$k(T) = \frac{3k^{1^3A'}(T) + k^{1^3A''}(T)\left(2 + e^{-227.71/T}\right)}{5 + 3e^{-227.71/T} + e^{-326.98/T}}, \quad (5)$$

where an adiabatic approximation has been made for the spin-orbit states, and $k^{2^3A''} = 0$. The results are compared with the experimental results of Lilenfeld & Richardson (1977) in Fig. 7. The present results are close to the experimental values for T=150-200 K, becoming a factor between 2 and 3 smaller at 300 K. According to the fit to the Arrhenius law shown in Fig. 7 the activation energy is ≈ 0.065 eV, while the potential energy barriers obtained here are lower, 0.043 and 0.058 for the $1^3A'$ and $1^3A''$ states, respectively. In fact, the rate constant obtained for $1\ ^3A'$ state alone is very close to the experimental value, changing the slope of the rate constant versus temperature. The disagreement at 300 K is attributed to inaccuracies of the $1,2^3A''$ excited electronic states. Also, since RPMD includes quantum effects such as tunneling and zero-point energy effects, we may conclude that the rate constant decreases with temperature, following an Arrhenius law. At the temperatures relevant in dense molecular clouds, T_k ~10 K, we may conclude that the CS + O reaction rate constant is negligible, below 10^{-15} cm^{3}s^{-1}.

5. Astrophysical implications

We have presented here a detailed theoretical study on the CS+O reaction, confirming the experimental data obtained at 150-400 K, and after a careful analysis at lower temperatures we find that the rate constant at 10K is negligible, below 10^{-15} cm^3 s^{-1}. Given the low value of the rate constant of the CS + O reaction at low temperature, this reaction does not seem to be able to explain the calculated overabundance of CS given by dense cloud models. A CS + O reaction rate close to 1×10^{-10} cm^{3}s^{-1} at 10 K, five orders of magnitude higher than our limit, would be needed to account for the observed CS abundances if no ad hoc depletion of sulfur is assumed. Besides the O + CS reaction, the chemical network for the destruction reactions of CS seems to us complete and relatively precise. The overestimation of CS does not seem to be due to an underestimation of the CS destruction reactions. Another hypothesis, previously put forward in the section above (CS chemical network) could be an overestimation of the CS production reactions. For a typical chemical evolution of the clouds corresponding to the observations, CS is mainly produced by neutral reactions, mainly S + CH and S + C_2. The rates for these two reactions in the model are close to those given by the capture theory, which may overestimate the value. A decrease in these rates would lead to a decrease in the production of CS because, despite their importance, the fluxes of these reactions are smaller than the fluxes of the S + H_3^+, S + OH, S + CH_3 reactions considering the CH, C_2, H_3^+, OH and CH_3 abundances given by the model (and for some of them by the observations) considering the physical conditions of the studied dark clouds. There is no experimental data or theoretical studies, to our knowledge, for the S + CH and S + C_2 reactions. Indeed, there is very little information on S + radical reactions in general. Flores et al. (2001) have performed a theoretical study of the S + C_2H reaction leading to a very high rate constant at low temperature, similar to the O + C_2H one (Georgievskii & Klippenstein 2011). Then, as the O + CH reaction is rapid at room temperature characteristic of a barrierless reaction (Messing et al. 1980), we may expect similar behavior for the S + CH reaction and a high rate constant at low temperature. An overestimation by more than a factor at least equal to 10 of the S + CH and S + C_2 reactions, required to reproduce the CS abundances, seems unlikely. Nevertheless, it is clear that theoretical and experimental studies are needed to better characterize S + radical reactions.

An additional problem comes from the fact that if the abundance of CS decreases, the abundance of HCS^+ would also decrease in typical dense clouds because in this case HCS^+ is mainly produced from CS. Then, as the measured abundances of HCS^+ are significantly higher than the modeled abundances, the decrease of CS will accentuate the disagreement. Either there is an unknown direct production (not from CS) of HCS^+ or the destruction of HCS^+ is overestimated. As the DR of HCS^+ is, by far, the main loss of HCS^+, a smaller value of the rate constant for this DR will increase the HCS^+ abundance. This DR has been

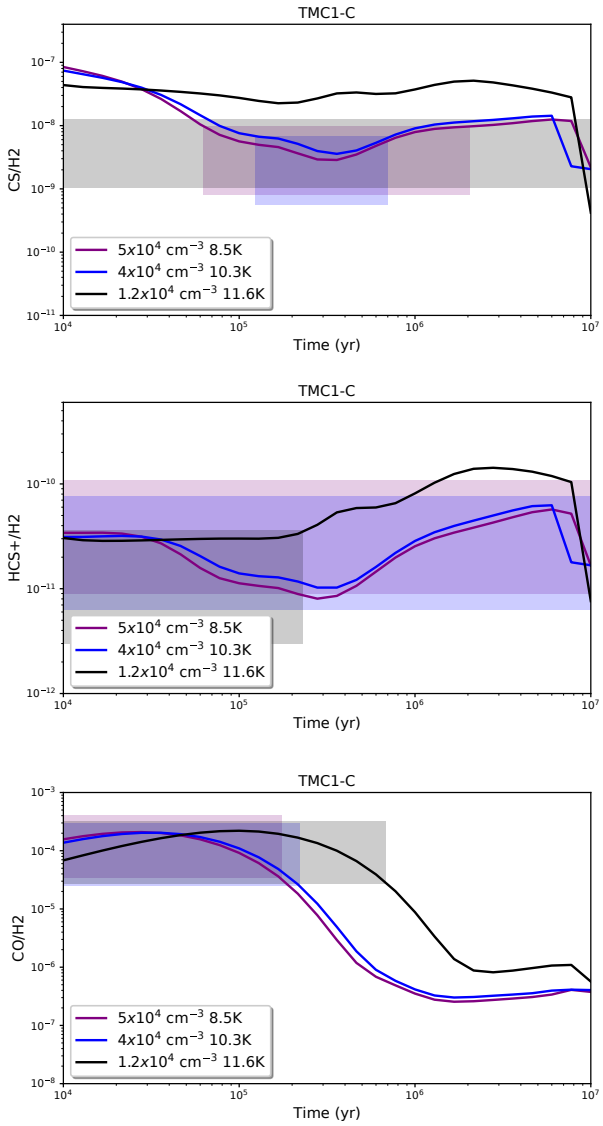

Fig. 8. Predicted abundances of gas-phase CS, HCS^+, and CO with respect to H_2 as a function of time. The curves correspond to the different physical conditions observed in the TMC1-C source with $\zeta_{H_2} = 10^{-16}$ s^{-1}. Each curve (density) corresponds to a different position of Table 3 in Fuente et al. (2019). Colored boxes represent the agreement with the observations. The abundance of sulfur with respect to H is depleted by a factor of 20 relative to the cosmic value.

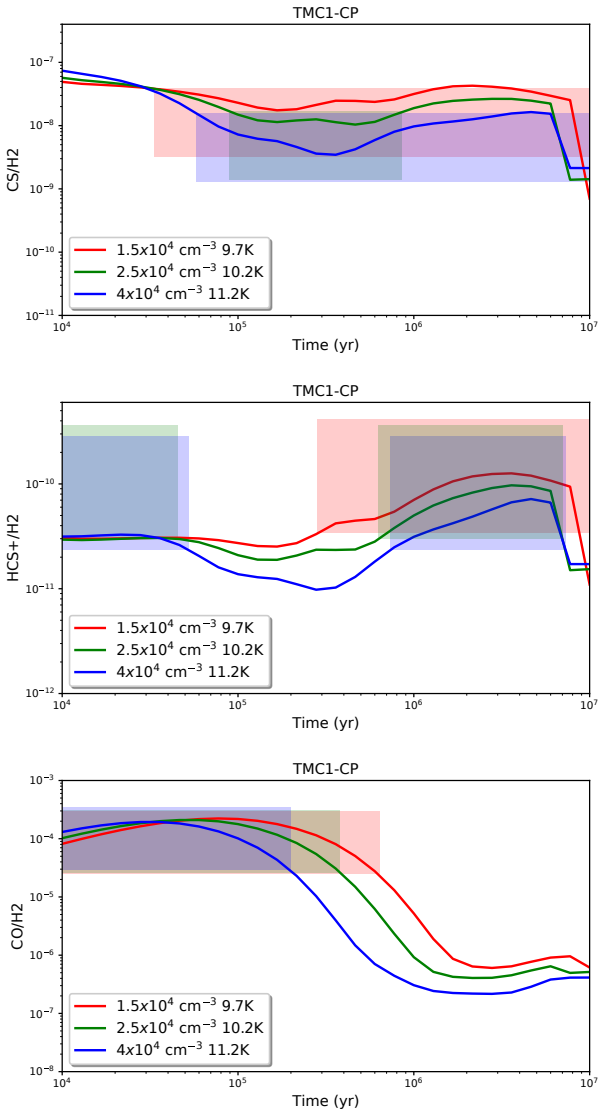

Fig. 9. Same as Fig. 8 for TMC1-CP.

experimentally studied by Montaigne et al. (2005) and there are no specific reasons to question this value. Nevertheless, there is only an experimental value and it can be noted that the DR of $HCNH^+$ (Adams et al. 1991; Semaniak et al. 2001; McLain & Adams 2009) and N_2H^+ (Shapko et al. 2020) vary greatly from one measurement to another. New experimental measurements of the DR of HCS^+ would be desirable to confirm the currently used value.

A crucial point in the modeling of sulfur compounds, in addition to the sulfur depletion factor, is their specific dependencies on the different physical conditions characterizing molecular clouds (density, cosmic-ray ionization rate, local temperature). We have detected different S-bearing species at different points along the dense clouds TMC 1-C, TMC 1-CP and TMC 1-NH3 (Fuente et al. 2019) within the program GEMS. Based on these data, we derived the gas physical conditions, $n(H_2)$ and T_k, and the CS column densities, by fitting the intensities of the observed J=1→0, 2→1 and 3→2 lines CS, $C^{34}S$ and ^{13}CS lines using the molecular excitation and radiative transfer code RADEX (van der Tak et al. 2007). During the fitting process, the ratios between the isotopologues were fixed to $N(^{12}CS)/N(^{13}CS)=60$, $N(C^{32}S)/N(C^{34}S)= 22.5$ (Gratier et al. 2016). The parameter space (T_k, $n(H_2)$ and N(CS)) was then explored following the Monte Carlo Markov Chain (MCMC) methodology with a Bayesian inference approach (Foreman-Mackey et al. 2012). This methodology allowed us to obtain an accurate estimate of the CS column density even if the CS lines are optically thick, providing that we had detections of the optically thin $C^{34}S$ and ^{13}CS lines. For other species such as H_2S and HCS^+ for which we had only one line observed (HCS^+ 1→0, o-H_2S $1_{1,0}$→$1_{0,1}$) , we obtained the column densities by assuming the values of T_k and $n(H_2)$ derived from the CS fitting and using RADEX. A detailed description of this procedure can be found in Fuente et al. (2019) and Navarro-Almaida et al. (2020). Moreover, Navarro-Almaida et al. (2020) modeled the abundances thus derived for TMC 1-CP and TMC 1-C and obtained a fairly good agreement for H_2S using an undepleted cosmic abundance

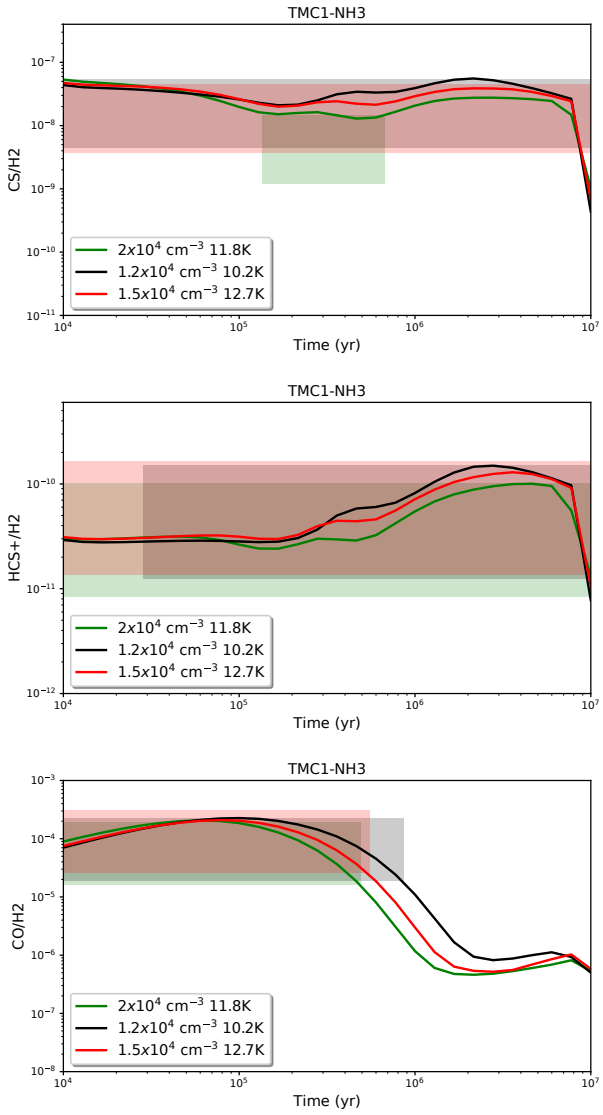

Fig. 10. Same as Fig. 8 for TMC1-NH3.

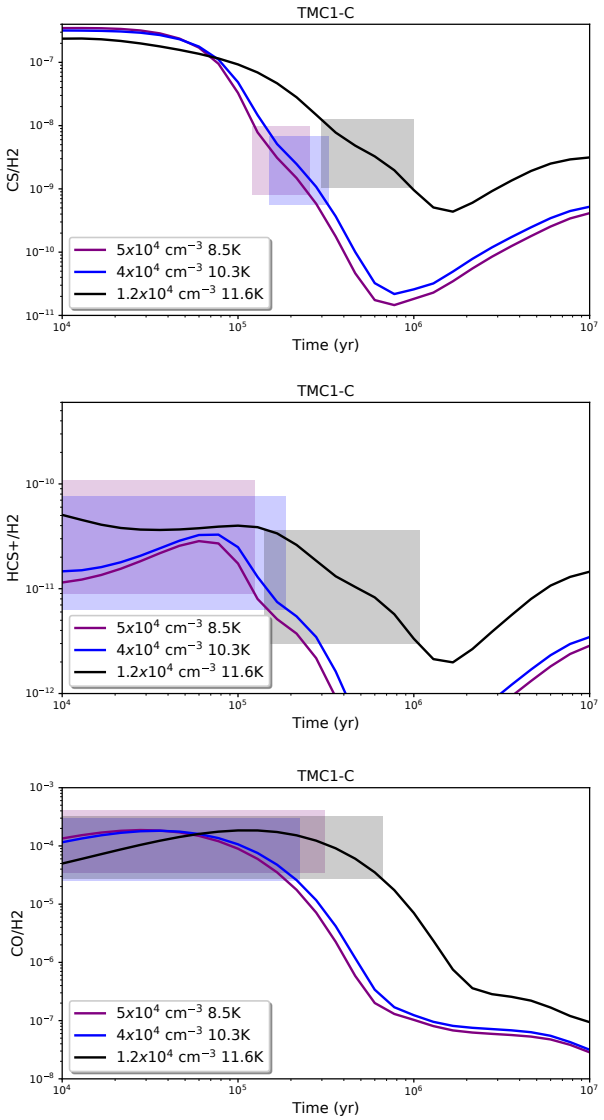

Fig. 11. Same as 8 same as Fig. 8 with ζ_{H_2} calculated for each visual extinction (see text and Indriolo & McCall 2012; Neufeld & Wolfire 2017).

with an uncertainty of a factor of 10, a chemical age of t=1 Myr, but with an overestimation of CS (Navarro-Almaida et al. 2020).

We resumed here this modeling without trying to reproduce H_2S but focusing only on CS and HCS^+ in TMC 1-CP, TMC 1-C and TMC 1-NH3. For this modeling we used an updated network from Vidal et al. (2017) and used the same temperatures, densities, incident UV flux, and visual extinction (A_V) of each observed region as Navarro-Almaida et al. (2020). For the cosmic-ray ionization rate for H_2, ζ_{H_2}, we used either the fixed value equal to $10^{-16}s^{-1}$ as determined by Fuente et al. 2019, or the values calculated as a function of A_V following the fit shown in Fig. 6 of Neufeld & Wolfire 2017).

$$log_{10}(\zeta_{H_2}) = -1.05 \times log_{10}(A_V) - 15.69 \quad (6)$$

This expression gives values of ζ_{H_2} are $\sim 10^{-17}$ s^{-1} for an A_V of 13 mag and $\sim 4\times10^{-17}$ s^{-1} for an A_V of 5 mag. These simulations are presented in Figs. 8 to 13 for CS, HCS^+, and CO. The abundance of CO has been calculated from observations of the $C^{18}O$ 1→0 line, and assuming N(CO)/N($C^{18}O$)=600 (see Fuente et al. 2019). The abundance of CO makes it possible to constrain quite strongly the maximum age of the clouds since CO is rapidly depleted under the physical conditions of these clouds. The colored boxes represent the period of time in which model predictions agree with observed abundance ratios at each position. An uncertainty of a factor of 2 is assumed for the observed abundances, which translates into an uncertainty of a factor of 4 in the molecular abundance ratios. As can be seen in Figs. 8, 9 and 10, the cosmic-ray ionization rate has a strong effect on the abundances of CS and HCS^+, and little effect on CO. For ζ_{H_2} = 10^{-16} s^{-1}, the CS profile is flat and the only way to obtain a good agreement between the observations and the model is to strongly deplete the sulfur (by a factor of 20 in the curves presented). In this case the agreement for CS and HCS^+ can be considered satisfactory, despite not very good as HCS^+ is underestimated for TMC 1-CP, while CO is also fairly well modeled. For lower values of ζ_{H_2}, such as those used in Figs. 11, 12 and 13, the CS profile is much more stepped at the typical ages of molecular clouds, with a similar shape to the CO curves showing the importance of depletion onto grains. In this case one can always find a cloud age that allows to reproduce CS regardless of the sulfur depletion factor. However, these ages are not compatible

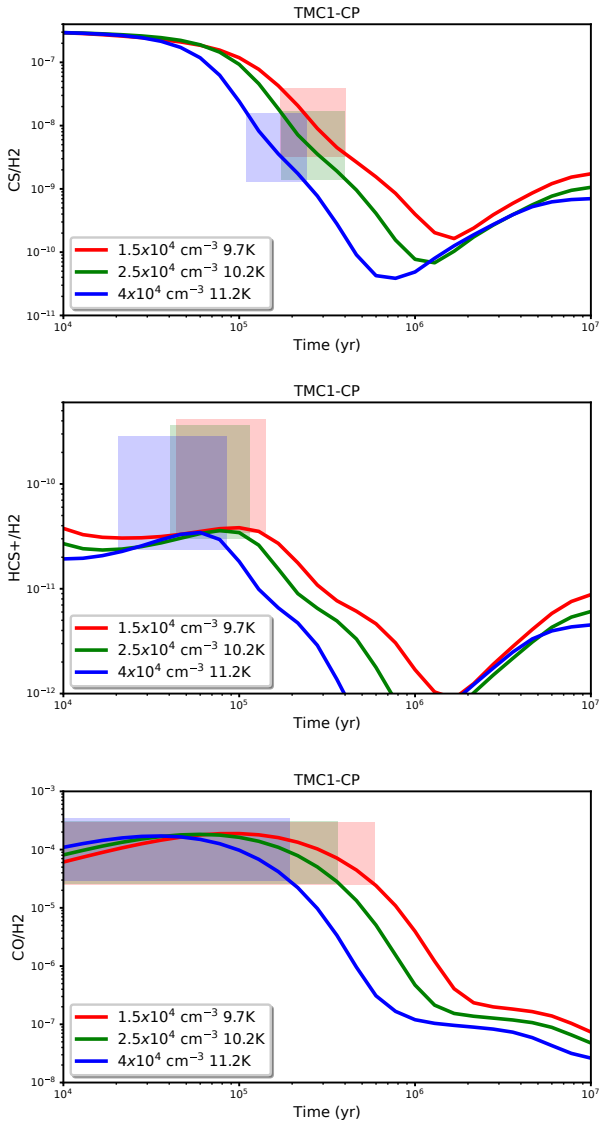

Fig. 12. Same as 9, with ζ_{H_2} calculated for each visual extinction..

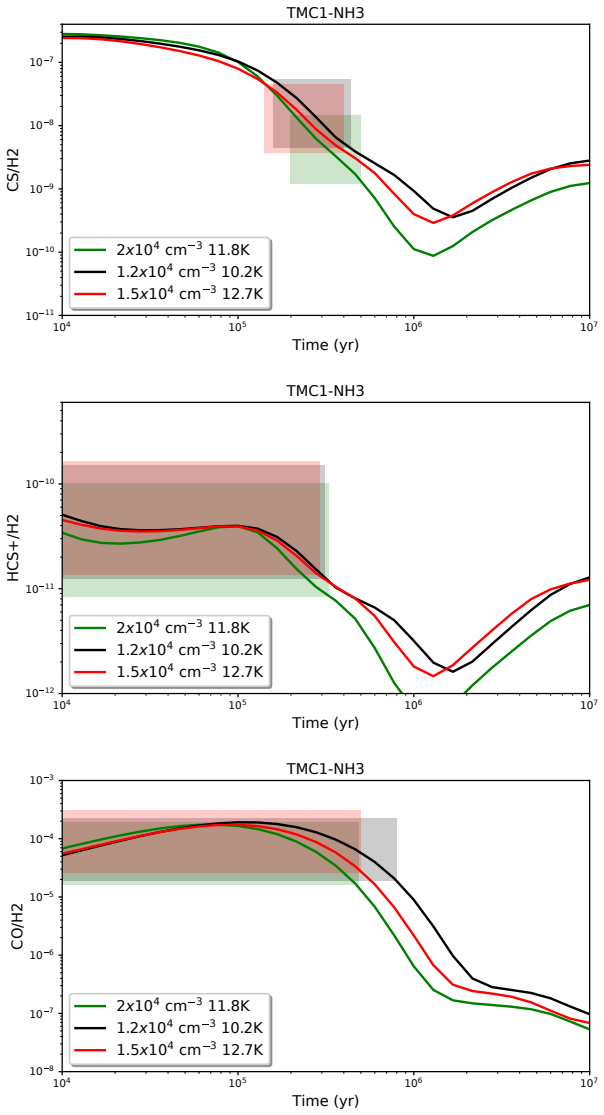

Fig. 13. Same as 10 with ζ_{H_2} calculated for each visual extinction.

with CO abundances when sulfur is not depleted, because they correspond to ages that are too large for which the CO is strongly depleted on the grains. An alternative, as shown in Figs. 8, 9 and 10, is to use a smaller sulfur abundance (factor 20 in the curves presented, similar to the case with a large cosmic-ray ionization rate). But in this case it is more difficult to reproduce the abundance of HCS^+ for ages where CS is reproduced. With such a sulfur depletion factor, the H_2S abundance would remain underestimated by a factor of >10, especially with a low cosmic-ray ionization rate.

Our study on the rate of the O + CS reaction removes one of the hypotheses for the overestimation of CS in the models versus the previous observations. The new analysis of GEMS observations using an updated chemical network shows the importance of the cosmic-ray ionization rate on sulfurated species in cold dark clouds. It would be desirable to complete the observational database with other important sulfur bearing species other than CS, HCS^+ and H_2S, in particular C_2S, C_3S, OCS and H_2CS to better estimate the importance of the cosmic-ray ionization rate and its coupling with the sulfur depletion factor. From the theoretical point of view, there is still room for significant improvement. Despite recent reviews on the chemistry of sulfur (Fuente et al. 2017; Vidal et al. 2017; Laas & Caselli 2019; Fuente et al. 2019; Navarro-Almaida et al. 2020; Shingledecker et al. 2020), the rates and branching ratios. of sulfur chemistry reactions are too poorly known which prevents the models from being really predictive. A substantial theoretical and experimental effort on the rates of neutral atomic sulfur reactions, on the branching ratios of S^+ reactions and on HCS^+ DR rate is needed if we hope to better understand the chemistry of sulfur in the interstellar medium.

6. Conclusions

The CS+O reaction has been proposed as a relevant CS destruction mechanism at low temperatures. Its reaction rate has been experimentally measured at temperatures of 150–400 K, but the extrapolation to lower temperatures is uncertain. In this study we have calculated the CS+O reaction rate at temperatures <150 K which are prevailing in clod dark clouds. We have performed *ab initio* calculations to produce the lower Potential Energy Surfaces (PES) of the CS +O system. These PES's are used to study the reaction dynamics, using several methods, classical, quantum

and semiclassical to eventually calculate the CS + O thermal reaction rates. In order to check the accuracy of our calculations, we compare the results with those obtained in laboratory over the T∼150−400 K range. We present a detailed theoretical study on the CS+O reaction which is in agreement with the experimental data, verifying the reliability of our approach. After a careful analysis at lower temperatures we find that the rate constant at 10 K is negligible, below 10^{-15} cm^3 s^{-1}, consistent with the extrapolation of experimental data using the Arrhenius expression.

We have modeled observations of CS and HCS^+ using an updated chemical network. We obtain a good fit of the CS, HCS^+ and SO abundances assuming a sulfur depletion of a factor of 20 and different chemical ages for each position within the cloud. Still, the H_2S abundance would remain underestimated by a factor of >10 unless we assume no sulfur depletion (S/H=1.5×10^{-5}). In spite of recent efforts to complete and update sulfur chemistry (Fuente et al. 2017; Vidal et al. 2017; Laas & Caselli 2019; Fuente et al. 2019; Navarro-Almaida et al. 2020; Shingledecker et al. 2020), there are still many uncertainties in the chemical network. A substantial theoretical and experimental effort on the rates of neutral atomic sulfur reactions, on the branching ratios of S^+ reactions and on the HCS^+ DR rate is needed if we hope to better understand the chemistry of sulfur in the interstellar medium. The observation of a wide inventory of S-bearing species is also necessary to better constrain the physical parameters, in particular the cosmic-ray ionization rate for H_2 and its variation along the cloud.

Acknowledgements. The research leading to these results has received funding from MICIU (Spain) under grants FIS2017-83473-C2, AYA2016-75066-C2-2-P, ESP2017-86582-C4-1-R, AYA2017-85111-P, PID2019-105552RB-C41 and PID2019-106235GB-I00. NB acknowledges the computing facilities by TUBITAK-TRUBA, and OR and AA acknowledge computing time at Finisterre (CESGA) and Marenostrum (BSC) under RES computational grants ACCT-2019-3-0004 and AECT-2020-1-0003. SPTM acknowledges the European Union's Horizon 2020 research and innovation program for funding support under agreement No 639450 (PROMISE).

References

Adams, N. G., Herd, C. R., Geoghegan, M., et al. 1991, J. Chem. Phys., 94, 4852
Aguado, A. & Paniagua, M. 1992, J. Chem. Phys., 96, 1265
Aguado, A., Paniagua, M., Lara, M., & Roncero, O. 1997, J. Chem. Phys., 106, 1013
Agúndez, M., Roueff, E., Le Petit, F., & Le Bourlot, J. 2018, A&A, 616, A19
Agúndez, M. & Wakelam, V. 2013, Chemical Reviews, 113, 8710
Anderson, D. E., Bergin, E. A., Maret, S., & Wakelam, V. 2013, ApJ, 779, 141
Bayet, E., Aladro, R., Martín, S., Viti, S., & Martín-Pintado, J. 2009, ApJ, 707, 126
Boisvert, R. F. 2015, The program was downloaded from http://gams.nist.gov/
Buckingham, A. D. 1967, Adv. Chem. Phys., 12, 107
Bulut, N., Aguado, A., Sanz-Sanz, C., & Roncero, O. 2019, J. Phys. Chem. A, 123, 8766
Calmonte, U., Altwegg, K., Balsiger, H., et al. 2016, MNRAS, 462, S253
Caselli, P., Walmsley, C. M., Zucconi, A., et al. 2002, ApJ, 565, 344
Clary, D. C. & Henshaw, J. P. 1987, Faraday Discuss. Chem. Soc., 84, 333
Craig, I. R. & Manolopoulos, D. E. 2004, J. Chem. Phys., 121, 3368
Craig, I. R. & Manolopoulos, D. E. 2005a, J. Chem. Phys., 122, 084106
Craig, I. R. & Manolopoulos, D. E. 2005b, J. Chem. Phys., 123, 034102
Davidson, E. R. 1975, J. Comp. Phys., 17, 87
de Boor, C. 1978, A practical guide to splines (Springer-Verlag, New York)
del Mazo-Sevillano, P., Aguado, A., Jiménez, E., Suleimanov, Y. V., & Roncero, O. 2019, J. Phys. Chem. Lett., 10, 1900
Denis-Alpizar, O., Stoecklin, T., Guilloteau, S., & Dutrey, A. 2018, MNRAS, 478, 1811
Dunning, T. H. & Jr. 1989, J. Chem. Phys., 90, 1007
Esplugues, G. B., Viti, S., Goicoechea, J. R., & Cernicharo, J. 2014, A&A, 567, A95
Flores, J. R., Estévez, C. M., Carballeira, L., & Juste, I. P. 2001, J. Phys. Chem. A, 105, 4716
Foreman-Mackey, D., Hogg, D. W., Lang, D., & Goodman, J. 2012
Fuente, A., Cernicharo, J., Roueff, E., et al. 2016, A&A, 593, A94
Fuente, A., Gerin, M., Pety, J., et al. 2017, A&A, 606, L3
Fuente, A., Navarro, D. G., Caselli, P., et al. 2019, A&A, 624, A105
Georgievskii, Y. & Klippenstein, S. J. 2011, in The Molecular Universe, ed. J. Cernicharo & R. Bachiller, Proc. IAU Symp. No. 280 (International Astronomical Union), 372
Goicoechea, J. R., Pety, J., Gerin, M., et al. 2006, A&A, 456, 565
Gómez-Carrasco, S., Roncero, O., & Aguado, A. 2020, in preparation
González, M., Hijazo, H., Novoa, J. J., & R, S. 1996, J. CHem. Phys., 105, 10999
Gratier, P., Majumdar, L., Ohishi, M., et al. 2016, ApJS, 225, 25
Gratier, P., Majumdar, L., Ohishi, M., et al. 2016, AstroPhys. J. S., 225, 25
Holdship, J., Viti, S., Jimenez-Serra, I., et al. 2016, MNRAS, 463, 802
Indriolo, N. & McCall, B. J. 2012, ApJ, 745, 91
Jiménez-Escobar, A. & Muñoz Caro, G. M. 2011, A&A, 536, A91
Kelly, G., Viti, S., Bayet, E., Aladro, R., & Yates, J. 2015, A&A, 578, A70
Kim, S., Lee, C. W., Gopinathan, M., et al. 2020, ApJ, 891, 169
Laas, J. C. & Caselli, P. 2019, A&A, 624, A108
Lapinov, A. V., Schilke, P., Juvela, M., & Zinchenko, I. I. 1998, A&A, 336, 1007
Le Gal, R., Öberg, K. I., Loomis, R. A., Pegues, J., & Bergner, J. B. 2019, ApJ, 876, 72
Lilenfeld, H. V. & Richardson, R. J. 1977, J. Chem. Phys., 67, 3991
Lique, F., Spielfiedel, A., & Cernicharo, J. 2006, A&A, 451, 1125
Martín, S., Martín-Pintado, J., Mauersberger, R., Henkel, C., & García-Burillo, S. 2005, ApJ, 620, 210
McGuire, P. & Kouri, D. 1974, J. Chem. Phys., 60, 2488
McKee, C. F. 1989, ApJ, 345, 782
McLain, J. L. & Adams, N. G. 2009, Planetary ans Space Science, 57, 1642
Messing, I., Carrington, T., Filseth, S. V., & Sadowski, C. M. 1980, Chem. Phys. Lett., 74, 56
Minissale, M., Dulieu, F., Cazaux, S., & Hocuk, S. 2016, A&A, 585, A24
Montaigne, H., Geppert, W. D., Semaniak, J., et al. 2005, ApJ, 631, 653
Navarro-Almaida, D., Le Gal, R., Fuente, A., et al. 2020, A&A, 637, A39
Neufeld, D. A., Godard, B., Gerin, M., et al. 2015, A&A, 577, A49
Neufeld, D. A. & Wolfire, M. G. 2017, ApJ, 845, 163
Pack, R. T. 1974, J. Chem. Phys., 60, 633
Padovani, M., Hennebelle, P., & Galli, D. 2013, A&A, 560, A114
Ruaud, M., Wakelam, V., & Hersant, F. 2016, MNRAS, 459, 3756
Ruffle, D. P., Hartquist, T. W., Caselli, P., & Williams, D. A. 1999, MNRAS, 306, 691
Semaniak, J., Minaev, B. F., Derkatch, A. M., et al. 2001, AstroPhys. J. Supplem. Ser., 135, 275
Shapko, D., Dohnal, P., Kassayová, M., et al. 2020, J. Chem. Phys., 152, 024301
Shingledecker, C. N., Lamberts, T., Laas, J. C., et al. 2020, AstroPhys. J., 52
Snell, R. L., Mundy, L. G., Goldsmith, P. F., Evans, N. J., I., & Erickson, N. R. 1984, ApJ, 276, 625
Suleimanov, Y. V., Aguado, A., Gómez-Carrasco, S., & Roncero, O. 2018, J. Phys. Chem. Lett., 9, 2133
Suleimanov, Y. V., Aoiz, F. J., & Guo, H. 2016, J. Phys. Chem. A, 120, 8488
Suleimanov, Y. V., Collepardo-Guevara, R., & Manolopoulos, D. E. 2011, J. Chem. Phys., 134, 044131
Tieftrunk, A., Pineau des Forets, G., Schilke, P., & Walmsley, C. M. 1994, A&A, 289, 579
van der Tak, F. F. S., Black, J. H., Schöier, F. L., Jansen, D. J., & van Dishoeck, E. F. 2007, A&A, 468, 627
Vastel, C., Quénard, D., Le Gal, R., et al. 2018, MNRAS, 478, 5514
Vidal, T. H. G., Loison, J.-C., Jaziri, A. Y., et al. 2017, MNRAS, 469, 435
Vidal, T. H. G. & Wakelam, V. 2018, MNRAS, 474, 5575
Wakelam, V., Ceccarelli, C., Castets, A., et al. 2005, A&A, 437, 149
Werner, H. J. & Knowles, P. J. 1988a, J. Chem. Phys., 89, 5803
Werner, H. J. & Knowles, P. J. 1988b, Chem. Phys. Lett., 145, 514
Werner, H.-J., Knowles, P. J., Knizia, G., Manby, F. R., & Schütz, M. 2012, WIREs Comput Mol Sci, 2, 242
Zanchet, A., Godard, B., Bulut, N., et al. 2013, ApJ, 766, 80
Zanchet, A., Roncero, O., González-Lezana, T., et al. 2009, J. Phys. Chem. A, 113, 14488
Zeimen, W. B., Klos, J., Groenenboom, G. C., & van der Avoird, A. 2003, J. Chem. Phys., 118, 7340
Zhao, B., Caselli, P., Li, Z.-Y., et al. 2016, MNRAS, 460, 2050